check for updates

ARTICLE

In Vitro and *in Silico* Insights on the Biological Activities, Phenolic Compounds Composition of *Hypericum perforatum* L. Hairy Root Cultures

Oliver Tusevski[1],*, **Marija Todorovska[1], Jasmina Petreska Stanoeva[2], Marina Stefova[2] and Sonja Gadzovska Simic[1]**

[1]Institute of Biology, Faculty of Natural Sciences and Mathematics, University "Ss. Cyril and Methodius", Skopje, 1000, Republic of North Macedonia

[2]Institute of Chemistry, Faculty of Natural Sciences and Mathematics, University "Ss. Cyril and Methodius", Skopje, 1000, Republic of North Macedonia

*Corresponding Author: Oliver Tusevski. Email: oliver.tusevski@pmf.ukim.mk

ABSTRACT

Three *Hypericum perforatum* hairy root lines (HR B, HR F and HR H) along with non-transformed roots were analyzed for phenolic compounds composition and *in vitro* enzyme inhibitory properties. *In silico* molecular modeling was performed to predict the interactions of the most representative phenolic compounds in HR clones with enzymes related to depression, neurodegeneration and diabetes. Chromatographic analyses revealed that HR clones represent an efficient source of quinic acid and hydroxybenzoic acids, epicatechin and procyanidin derivatives, quercetin and kaempferol glycosides, as well numerous xanthones. *In vitro* antidepressant activity of HR extracts through monoamine oxidase A (MAO-A) inhibition was attributed to the production of oxygenated and prenylated xanthones. The neuroprotective potential of HR extracts was related to the accumulation of quercetin 6-*C*-glucoside, epicatechin, procyanidins and γ-mangostin isomers as potential inhibitors of acetylcholinesterase (AChE) and butyrylcholinesterase (BChE). Vanillic acid and prenylated xanthones in HR clones as promising inhibitors of tyrosinase additionally contributed to the neuroprotective activity. Five preeminent xanthones in HR (γ-mangostin, mangiferin, garcinone C, garcinone E and 1,3,7-trihydroxy-6-metoxy-8-prenyl xanthone) along with the flavonol quercetin 6-*C*-glucoside effectively inhibited α-amylase and α-glucosidase indicating the antidiabetic properties of HR extracts. Transgenic roots of *H. perforatum* can be exploited for the preparation of novel phytoproducts with multi-biological activities.

KEYWORDS

Biological activities; hairy roots; *Hypericum perforatum*; molecular docking; phenolic compounds

1 Introduction

Hypericum perforatum L. (St. John's wort) is a widely investigated medicinal species due to its unique spectrum of secondary metabolites with various pharmacological properties. The extracts from *H. perforatum* contained numerous secondary metabolites that exhibited antidepressant, antibacterial, antifungal, antiviral, anti-inflammatory and anticancer activities [1]. The most representative compounds such as hypericins (hypericin and pseudohypericin), hyperforins (hyperforin and adhyperforin) and

flavonoids (quercetin, kaempferol, rutin, quercitrin and hyperoside) have been synthesized in the aerial parts of the plant [2,3]. Flowering parts of *H. perforatum* have been widely studied due to the growing demand of standardized phytopharmaceutical preparations, the limited area of occurrence, seasonal harvesting, loss of biodiversity, as well as qualitative and quantitative variations of bioactive metabolites [4]. The phytochemical variability of *H. perforatum* field-grown plants has been strongly influenced by genetic, physiological, developmental, ecological and environmental factors [5,6]. For these reasons, it is difficult to produce chemically consistent *H. perforatum* plants and to obtain high-quality standardized extracts containing stable quantities of hypericins, hyperforins, and flavonoids.

Despite the extensive phytochemical and pharmacological investigations of Hyperici herba, the presence of bioactive compounds in roots is not yet fully known. In the last few years, root extracts of *H. perforatum* have been recognized as a new source of xanthones with potential biological properties [3,7,8]. Our recent study revealed that *H. perforatum* wild-growing roots have a capability to accumulate hydroxycinnamic acids, catechins and xanthones as promising compounds for the treatment of bacterial and fungal diseases, depression, neurodegeneration and diabetes [3]. The xanthones from root extracts have also been shown as efficient compounds towards various fungal pathogens [7]. However, commercial application of root-derived preparations is still limited due to the differences in xanthone contents that are influenced by soil properties, altitude and plant developmental stage [8]. These limitations lead to the establishment of *in vitro* strategies for large-scale biomass production of *H. perforatum* roots with stable content of xanthones.

To the best of our knowledge, *H. perforatum* root cultures are characterized by high proliferation rate, morphogenetic potential and genetic stability that make them an efficient system for secondary metabolite production [9,10]. Taking into account this consideration, *H. perforatum* root cultures have been widely used as a promising biotechnological system for xanthone production [8,11]. The xanthone accumulation in *Hypericum* root cultures has been improved by standardization of inoculum density, cultivation time, as well as dark/light conditions [10–12]. Several strategies have also been applied to enhance xanthone production in root cultures including optimization of culture medium, exogenous application of elicitors and genetic manipulation. Recent studies have been focused on xanthone overproduction in *H. perforatum* root cultures upon elicitation with auxins, carboxymethylchitosans, chitosan oligosaccharides and acetic acid [10,13,14]. These elicitation experiments showed that root cultures can lose their morphogenetic potential resulting in poor or transient xanthone accumulation [11,14]. Although the optimization of culture medium and elicitation represented a key prerequisite for enhanced xanthone production, the productivity is still far away for bioprocessing application. Nowadays, genetic transformation technology has opened new avenues to improve the content of existing secondary metabolites and to enhance the production of new uncharacterized bioactive compounds in root cultures.

In the recent past, the application of genetic transformation as a potential strategy for increased production of secondary metabolites in *H. perforatum* has limited success due to the lack of an efficient transformation system [15]. Among the gene transfer methods, *Agrobacterium rhizogenes*-mediated transformation has been widely used for successful induction of *Hypericum* hairy root (HR) cultures [12,16–18]. All these studies showed that *Hypericum* transformation with various *A. rhizogenes* strains represented an efficient strategy for establishment of HR cultures that accumulated significant amounts of xanthones [12,17,18]. These HR cultures have been shown as a prominent source of various secondary metabolites due to their fast auxin-free growth and biomass accumulation, as well as great genetic and biochemical stability [17,19]. In this context, *H. perforatum* HR exhibited a strong potential for the production of quinic acid derivatives, flavonoids and xanthones. Our previous studies clearly showed a great heterogeneity in the growth and phenotype, production of phenolic compounds, and antioxidant and antibacterial properties among different *H. perforatum* HR clones [18,20]. In addition, *H. tomentosum* and *H. tetrapterum* HR clones have been shown to accumulate a variety of xanthones with antifungal

activities [12]. The clonal differences of *Hypericum* HR lines could be related to the genetic variations induced by pRiA4 T-DNA, such as heterogeneity in *rol* genes expression or their copy number integrated into the *H. perforatum* genome [19,21]. Thus, the screening of HR lines originated from independent transformation events would be of great interest to selecting transgenic clones with significant amounts of bioactive metabolites. Our recent study was directed on the selection of superior *H. perforatum* HR clones with respect to biomass proliferation, total phenolic compounds production, as well non-enzymatic and enzymatic antioxidant status [20]. Nevertheless, those *H. perforatum* HR lines have never been the subject of extensive phytochemical profiling and screening of biological activities through *in vitro* enzyme inhibitory assays.

This study reports for the first time a detailed phenolic profile and *in vitro* biological activities of selected *H. perforatum* HR clones. In addition, *in silico* molecular docking technique was used to evaluate the mechanism of phenolics' inhibitory activities against several enzymes of clinical importance. For the realization of the main objectives, HR extracts were evaluated from the following aspects:

(1) chromatographic analysis of phenolic compounds by HPLC/DAD/ESI-MS^n;
(2) *in vitro* inhibitory potential against key enzymes associated with depression (monoamine oxidase-A), neurodegeneration (acetylcholinesterase, butyrylcholinesterase and tyrosinase) and diabetes (α-amylase and α-glucosidase);
(3) *in silico* molecular docking study of the interactions between phenolic compounds and target enzymes.

2 Materials and Methods

2.1 Plant Material and Extract Preparation

Seeds from *H. perforatum* were collected from field-grown plants in the National Park Pelister (Republic of North Macedonia) at about 1394 m. Voucher specimen number (060231) of *H. perforatum* is deposited in the Herbarium at the Faculty of Natural Sciences and Mathematics, University "Ss. Cyril and Methodius" in Skopje, Republic of North Macedonia (MKNH). The seeds were washed with 70% ethanol for 30 s, surface sterilized with 1% NaOCl for 15 min, rinsed 3 times in sterile deionized water and cultured on MS/B$_5$ medium. *In vitro* grown seedlings were maintained in a growth chamber at $25 \pm 1°C$ under a photoperiod of 16 h light, irradiance at 50 μmol m^2 s^{-1} and 50% to 60% relative humidity.

The culture conditions and transformation protocol for establishment of *H. perforatum* HR were previously described [17]. Briefly, root segments from one-month-old *in vitro* grown seedlings of *H. perforatum* were used for transformation experiments with *Agrobacterium rhizogenes* strain A4. In our recent study, fifteen HR clones (HR A-HR O) were evaluated for biomass accumulation, total phenolic compounds production and antioxidant state [20]. Two superior clones denoted as HR B and HR F, one randomly selected line HR H, as well non-transformed roots (NTR) were presently used for the determination of phenolic profile and enzyme inhibitory potential.

The HR and NTR were harvested from solid media and washed with distilled water. Then, root samples were air dried in darkness, ground to powder by a laboratory mill, and stored in airtight containers for further analysis. The root extracts for identification and quantification of phenolic compounds were prepared when powdered root material (0.2–0.5 g) was homogenized with 80% (v/v) CH$_3$OH in an ultrasonic bath for 30 min at 4°C [4]. Thereafter, methanolic extracts were centrifuged at 13000 rpm for 20 min and the supernatants were used for HPLC/DAD/ESI-MS^n analysis. For determination of enzyme inhibitory activities, root methanolic extracts were evaporated under vacuum at room temperature. Then, dried extracts were dissolved in dimethyl sulfoxide (DMSO) and three extract concentrations (250, 150 and 50 μg·mL^{-1}) were used for evaluation of *in vitro* enzyme inhibitory properties. Those extract

concentrations considered as physiologically relevant were selected in order to obtain data from 0% to 100% enzyme inhibitory activities [3].

2.2 HPLC/DAD/ESI-MSn Analysis of Phenolic Metabolites

The identification and quantitative analysis of phenolic compounds in root extracts was performed on Agilent Technologies 1,100 series high pressure liquid chromatography (HPLC) system equipped with a binary pump, autosampler, degasser, diode array and mass detector in series. The separations of phenolic metabolites were performed using reverse-phase Zorbax Eclipse XDB-C18 column (150 mm × 4.6 mm, 5 μm particle size) that was maintained at 38°C. The mobile phase consisted of eluent A: water-formic acid (99:1, v/v) and eluent B: CH_3OH. The solvents used for mobile phase were LC-MS grade purchased from Sigma-Aldrich Chemie GmbH (Steinheim, Germany). Multilinear gradient program was used: 10% B (0–20 min), 20% B (20–30 min), 35% B (30–50 min), 50% B (50–70 min), 80% B (70–80 min) and continued with 100% B for a further 10 min. Flow rate of the mobile phase was set at 0.4 mL·min^{-1} and the injection volume of all extracts and standards was 10 μL. The reference standards of chlorogenic acid, catechin, epicatechin, quercetin, kaempferol and mangiferin were HPLC grade with 95%–98% purity (Sigma-Aldrich Chemie GmbH, Steinheim, Germany). Those reference compounds were dissolved in methanol and kept at 4°C until analyses. Spectral data of the sample peaks were collected in the range 190–600 nm and chromatograms were monitored at 350 nm for flavonols, 330 nm for phenolic acids, as well at 280 and 260 nm for flavan-3-ols and xanthones, respectively. The acquisition of the MS data was performed using ion-trap mass spectrometer (Agilent G2449A) equipped with electrospray ionization (ESI) source and operated by LCMSD software. The mass detector conditions were set as follows: ESI negative ionization mode; full scan mode from 100 to 1200 m/z; capillary temperature and voltage of 350°C and 4000 V, respectively and nitrogen flow rate of 12 L·min^{-1}. Fragmentation was performed by collision induced dissociation using helium as a collision gas. Tentative identification of peaks was based on the retention time, UV/Vis spectral data, m/z values of the molecular ions, fragmentation patterns and previously reported data [3,17,18,22,23].

2.3 In Vitro Biological Activity Evaluation

The comprehensive protocols for antidepressant activity through monoamine oxidase-A (MAO-A) inhibition, neuroprotective activity through acetylcholinesterase (AChE), butyrylcholinesterase (BChE) and tyrosinase inhibition, as well as antidiabetic activity through α-amylase and α-glucosidase inhibition were reported in our previous study [3].

The reaction mixture for MAO-A inhibition consisted of plant extract, 0.2 M potassium phosphate buffer (pH 7.2), chromogenic solution (1 mM vanillic acid and 0.5 mM 4-aminoantipyrine containing 5 U·mL^{-1} horseradish peroxidase), 3 mM tyramine and 5 U·mL^{-1} MAO-A (human recombinant, expressed in baculovirus infected BTI insect cells). The samples were incubated at 37°C for a period of 10 min and the increase in absorbance was monitored at 492 nm.

Cholinesterase inhibitory activity was performed by mixing of plant extract, 50 mM Tris-HCl buffer (pH 8) with 0.1% bovine serum albumin, 3 mM of DTNB and 0.26 U·mL^{-1} AChE from *Electrophorus electricus* (type VI-S) or BChE from equine serum. The reaction was initiated by addition of 15 mM acetylthiocholine iodide for AChE or butyrylthiocholine chloride for BChE and the absorbance was monitored at 405 nm for a period of 5 min.

The reaction mixture for tyrosinase inhibitory activity consisted of plant extract, 50 mM sodium phosphate buffer (pH 6.8) and 31.3 U·mL^{-1} mushroom tyrosinase. After incubation at 37°C for 10 min, the reaction was initiated by addition of 2.5 mM 3,4-dihydroxy L-phenylalanine (L-DOPA) and the increase in absorbance at 475 nm was monitored for a period of 12 min.

For α-amylase inhibitory activity, plant extract was incubated with 0.5 mg·mL^{-1} enzyme from *Aspergillus oryzae* at room temperature for 10 min. Thereafter, 0.5% starch in 50 mM sodium phosphate buffer (pH 6.8) was added to the reaction mixture and samples were incubated at room temperature for 10 min. The reaction was stopped by addition of DNS reagent (1% 3,5-dinitro salicylic acid and 12% sodium potassium tartrate in 2 M NaOH) and samples were incubated at 95°C for 5 min. After cooling at room temperature, the samples were diluted with buffer and the absorbance was measured at 540 nm.

The reaction mixture for α-glucosidase inhibition consisted of plant extract, 50 mM sodium phosphate buffer (pH 6.8) and 0.26 U·mL^{-1} enzyme from *Saccharomyces cerevisiae* was incubated at 37°C for 15 min. Thereafter, 3 mM *p*-nitrophenyl-α-D-glucopyranoside was added to the reaction mixture and samples were further incubated at 37°C for 15 min. The reaction was stopped by addition of 0.2 M Na_2CO_3 and the absorbance was measured at 405 nm.

The percentages of inhibition by tested extracts were compared with specific enzyme inhibitors, such as 2,4-dichlorophenol (2,4-DCP) for MAO, eserine for AChE and BChE, kojic acid for tyrosinase and acarbose for α-amylase and α-glucosidase.

2.4 Molecular Modelling

2.4.1 Enzyme Preparation

The crystallographic structures of six enzymes evaluated in this study were downloaded from the Protein Data Bank RSCB PDB [24]. The docking experiments were performed with the following enzyme/inhibitor complexes: MAO-A/harmine (pdb: 2Z5X), AChE/tacrine-nicotinamide (pdb: 4X3C), BChE/tacrine (pdb: 4BDS), tyrosinase/tropolone (pdb: 2Y9X), α-amylase/*p*-nitrophenyl-α-D-maltoside (pdb: 1VAH) and α-glucosidase/maltose (pdb: 3AXI) [25–30]. The raw crystal structures of the enzymes were prepared by AutoDock Tools 4.2 [31] that involves elimination of all water molecules, ligands and co-factors, addition of Kollman united-atom partial charges for neutralization of enzymes and merging of non-polar hydrogens. It is worth mentioning that Cu ions from the active site of tyrosinase enzyme were manually assigned to +2, since AutoDock program can not apply charge to metals. The web application MolProbity was used to generate correct hydrogen bond network for all tested enzymes [32] and the final enzyme structures were saved in pdbqt format by AutoDock tools 4.2.

2.4.2 Ligand Preparation

The molecular docking study was performed with vanillic acid, epicatechin, quercetin 6-*C*-glucoside, mangiferin and γ-mangostin as the most abundant and representative phenolic compounds from *H. perforatum* HR extracts. The ligand molecules were downloaded from PubChem online database [33] or sketched in ChemSketch software [34] and then subjected to automatic 3D Structure Optimization (2018.2.1). Atomic charge and potential of the ligands were computed using VEGA ZZ program (3.1.2) using TRIPOS force field along with Gasteiger charges [35]. After this optimization procedure, the ligand structures were saved in pdbqt format by AutoDock tools 4.2.

2.4.3 Molecular Docking

AutoDock 4.2 software package was used as an automated docking tool to predict the molecular interactions between the representative ligands and enzyme receptors using the Lamarckian Genetic Algorithm [31]. Standard docking protocol for rigid protein and flexible ligands was implemented with 10 independent runs per ligand. AutoGrid 4.2 program was used to calculate grid maps of 60 × 60 × 60 (number of points in x-, y- and z-axes for tested enzymes) with 0.375 Å distance between grid points. The best ligand binding conformation was selected according to the lowest binding energy and inhibition constant, as well the type of interaction and intermolecular distance between the ligand atoms and enzyme amino acid residues. The most accurate results were analyzed using the Discovery Studio Visualizer 16.1 (Accelrys, San Diego, CA, USA).

2.5 Statistical Analyses

The results for phenolic compound contents and *in vitro* enzyme inhibition were expressed as mean values with standard deviation. The statistical analyses were performed using the software program STATISTICA for Windows (v. 8.0; StatSoft Inc., Tulsa, USA). Mean values were compared by one-way ANOVA analysis of variance. The significant differences ($p < 0.05$) were *Post hoc* statistically evaluated using Duncan's multiple range test.

3 Results

3.1 Chromatographic Analysis of Phenolic Compounds

Phenolic acids. Three phenolic acids denoted as F2, F10 and F12, along with F1 identified as quinic acid were detected in root extracts (Table 1). Vanillic acid (F10) was quantified in comparable amounts in all tested extracts. Quinic acid was *de novo* synthesized in all HR clones, while vanillic acid derivative (F2) was exclusively found in HR B and HR F. The amount of F1 in HR H was significantly higher compared to HR B and HR F. Syringic acid (F12) was evidenced only in HR H and NTR. The total content of phenolic acids did not vary markedly among the HR clones and only HR H showed significantly higher value in comparison to NTR cultures.

Table 1: Phenolic compounds quantification in *H. perforatum* root extracts

Peak	Phenolic compounds	t_R (min)	NTR	HR B	HR F	HR H
Phenolic acids						
F1	Quinic acid	6.50	n.d.	0.18 ± 0.01^a	0.15 ± 0.01^a	0.30 ± 0.02^b
F2	Vanillic acid derivative	17.81	n.d.	0.44 ± 0.03^a	0.43 ± 0.02^a	n.d.
F10	Vanillic acid	34.31	0.79 ± 0.04^b	0.65 ± 0.03^a	0.86 ± 0.05^b	0.78 ± 0.10^{ab}
F12	Syringic acid	37.88	0.50 ± 0.03^a	n.d.	n.d.	0.63 ± 0.04^b
Total			1.29 ± 0.07^a	1.27 ± 0.07^a	1.44 ± 0.08^a	1.71 ± 0.16^b
Flavan-3-ols						
F3	*trans*-Cinnamic acid derivative of catechin/(epi)catechin	25.98	n.d.	1.67 ± 0.21^b	1.24 ± 0.11^a	1.59 ± 0.18^b
F4	B-type procyanidin dimer	27.89	0.52 ± 0.04^a	1.38 ± 0.11^b	3.30 ± 0.27^c	0.60 ± 0.03^a
F5	B-type procyanidin dimer	30.66	0.67 ± 0.07^a	0.83 ± 0.07^a	2.34 ± 0.19^b	n.d.
F6	Procyanidin trimer	31.08	1.15 ± 0.12^a	1.49 ± 0.16^b	3.21 ± 0.26^c	n.d.
F7	B-type procyanidin dimer	31.26	0.53 ± 0.06^a	0.62 ± 0.05^a	1.50 ± 0.12^b	n.d.
F8	(epi)catechin	32.02	3.94 ± 0.32^b	5.88 ± 0.61^c	9.08 ± 1.02^d	1.23 ± 0.09^a
F9	Galloylquinic acid	33.27	0.08 ± 0.01	n.d.	n.d.	n.d.
F14	B-type procyanidin dimer	39.45	0.11 ± 0.01	n.d.	n.d.	n.d.
F15	Biflavanoid with one catechin/(epi)catechin monomer	40.52	n.d.	0.48 ± 0.06^b	0.18 ± 0.02^a	0.16 ± 0.02^a
F16	Biflavanoid with one catechin/(epi)catechin monomer	42.77	n.d.	n.d.	0.78 ± 0.08^b	0.21 ± 0.02^a
Total			7.00 ± 0.63^b	12.35 ± 1.28^c	22.35 ± 2.07^d	3.79 ± 0.34^a
Flavonol glycosides						
F11	Quercetin 6-*C*-glucoside	36.26	0.37 ± 0.05^a	1.07 ± 0.12^c	1.40 ± 0.17^d	0.64 ± 0.09^b
F13	Kaempferol 6-*C*-glucoside	38.13	0.17 ± 0.02^a	0.88 ± 0.11^b	0.81 ± 0.10^b	n.d.
Total			0.54 ± 0.07^a	1.95 ± 0.33^b	2.21 ± 0.27^b	0.64 ± 0.09^a

Note: Contents of phenolics are expressed as milligrams per gram dry weight (mg·g^{-1} DW ± SD). NTR: non-transformed roots; HR B, HR F, HR H: hairy root clones; n.d.: not detected; t_R: retention time. Values in one row marked with different lower-case letters denoted significant differences between samples ($p < 0.05$).

Flavan-3-ols. Ten compounds from the group of flavan-3-ols (F3-F9, F14-F16) were identified in NTR and HR extracts (Table 1). Procyanidin dimer B-type (F4) and (epi)catechin (F8) were detected in all root samples. The (epi)catechin was found as the most representative flavan-3-ol in the analyzed samples. This compound was found in significantly higher amounts in HR B and HR F clones compared to control roots. The clone HR F produced markedly higher amount of F4 compared to HR B, HR H and NTR. Galloylquinic acid (F9) and another B-type procyanidin dimer (F14) were found in minor amounts only in NTR. *Trans*-cinnamic acid derivative of catechin/(epi)catechin (F3) and biflavanoid with one catechin/(epi)catechin monomer (F15) were *de novo* synthesized in all HR clones. Notably, HR B was selected as the most prominent clone for the production of F3 and F15. Another biflavanoid with one catechin/(epi)catechin monomer (F16) was confirmed only in two clones and its content was significantly higher in HR F than in HR H. Two B-type procyanidin dimers (F5 and F7) and procyanidin trimer (F6) were detected in all samples except for HR H. The HR F was selected as a superior clone with markedly higher production of F5, F6 and F7 compared to NTR and HR B. Taking into account the contents of total flavan-3-ols, HR F was shown as the richest source of these compounds.

Flavonol glycosides. Two flavonol glycosides, quercetin 6-*C*-glucoside (F11) and kaempferol 6-*C*-glucoside (F13) were presented in root samples (Table 1). Transgenic clones contained significantly higher amounts of F11 compared to NTR. The contents of F13 were markedly elevated in HR F and HR B in comparison to control roots. Regarding the total contents, HR F and HR B were shown as greater producers of flavonol glycosides (from 3- to 4-fold) compared to HR H and control roots.

Xanthones. Thirty-eight xanthones were confirmed in *H. perforatum* transgenic and control roots, while nine of them were presented as xanthone derivatives (Table 2). The xanthones exclusively detected in NTR extracts were classified in two groups according to their quantification data. The first group of xanthones with quantities from 0.3 to 0.8 mg·g^{-1} DW was represented by 1,3,6-trihydroxy-7-methoxy-8-prenyl xanthone (X19), 1,3,7-trihydroxy-2-(2-hydroxy-3-methyl-3-butenyl)-xanthone (X21) and trihydroxy-1-metoxy-*C*-prenyl xanthone (X24). The second group of xanthones (up to 0.3 mg·g^{-1} DW) included 2-isoprenylemodin isomer (X12), 1,3,6,7-tetrahydroxyxanthone dimer (X14), 1,3,7-trihydroxy-6-methoxy-8-prenyl xanthone (X18) and 5-*O*-methylcelebixanthone (X26).

Table 2: Xanthones quantification in *H. perforatum* root extracts

Peak	Xanthones	t_R (min)	NTR	HR B	HR F	HR H
X1	Linixanthone C	32.25	n.d.	n.d.	n.d.	0.25 ± 0.03
X2	Xanthone derivative 1	32.60	0.29 ± 0.03^a	0.30 ± 0.02^a	0.91 ± 0.06^c	0.54 ± 0.06^b
X3	Mangiferin	33.92	1.09 ± 0.11^c	0.53 ± 0.04^a	1.11 ± 0.14^c	0.85 ± 0.09^b
X4	Xanthone derivative 2	35.15	n.d.	1.83 ± 0.12^a	2.20 ± 0.19^b	n.d.
X5	Xanthone derivative 3	35.79	n.d.	1.63 ± 0.18^a	1.71 ± 0.20^a	n.d.
X6	Homomangiferin	36.59	n.d.	2.99 ± 0.34	n.d.	n.d.
X7	2-Isoprenylemodin	37.87	n.d.	n.d.	n.d.	0.17 ± 0.02
X8	Linixanthone B	38.97	0.45 ± 0.06^a	n.d.	n.d.	1.30 ± 0.15^b
X9	Isomangiferin	41.70	n.d.	n.d.	n.d.	0.81 ± 0.07
X10	Xanthone derivative 4	43.34	0.39 ± 0.05^a	0.75 ± 0.09^b	0.99 ± 0.07^c	0.87 ± 0.09^{bc}
X11	Linixanthone C isomer	46.41	0.27 ± 0.04^a	n.d.	0.34 ± 0.04^a	n.d.
X12	2-Isoprenylemodin isomer	48.17	0.14 ± 0.01	n.d.	n.d.	n.d.
X13	Xanthone derivative 5	50.73	n.d.	0.18 ± 0.02	n.d.	n.d.
X14	1,3,6,7-Tetrahydroxyxanthone dimer	51.09	0.23 ± 0.01	n.d.	n.d.	n.d.

(Continued)

Table 2 (continued)

Peak	Xanthones	t_R (min)	NTR	HR B	HR F	HR H
X15	Xanthone derivative 6	57.15	n.d.	0.44 ± 0.02^c	0.19 ± 0.01^b	0.11 ± 0.01^a
X16	γ-Mangostin isomer	72.89	n.d.	n.d.	0.17 ± 0.02	n.d.
X17	1,3,5,6-Tetrahydroxyxanthone 8-prenyl xanthone	73.65	0.72 ± 0.08	n.d.	0.22 ± 0.02	n.d.
X18	1,3,7-Trihydroxy-6-methoxy-8-prenyl xanthone	73.82	0.14 ± 0.01	n.d.	n.d.	n.d.
X19	1,3,6-Trihydroxy-7-methoxy-8-prenyl xanthone	74.63	0.48 ± 0.02	n.d.	n.d.	n.d.
X20	3,6-Dihydroxy-1,5,7-trimethoxy-xanthone	74.67	n.d.	0.05 ± 0.01	n.d.	n.d.
X21	1,3,7-Trihydroxy-2-(2-hydroxy-3-methyl-3-butenyl)-xanthone	75.17	0.32 ± 0.04	n.d.	n.d.	n.d.
X22	1,3,6,7-Tetrahydroxyxanthone 8-prenyl xanthone	76.65	0.93 ± 0.10^c	0.46 ± 0.06^b	0.14 ± 0.01^a	n.d.
X23	1,3,7-Trihydroxy-6-methoxy-8-prenyl xanthone isomer	76.91	n.d.	1.24 ± 0.14^b	0.40 ± 0.05^a	0.31 ± 0.02^a
X24	Trihydroxy-1-metoxy-C-prenyl xanthone	77.42	0.77 ± 0.09	n.d.	n.d.	n.d.
X25	Paxanthone	78.37	0.89 ± 0.11^c	0.23 ± 0.03^a	0.43 ± 0.03^b	n.d.
X26	5-*O*-Methylcelebixanthone	79.02	0.12 ± 0.01	n.d.	n.d.	n.d.
X27	γ-Mangostin isomer	79.48	0.30 ± 0.02^a	0.39 ± 0.05^a	1.37 ± 0.16^c	0.52 ± 0.04^b
X28	γ-Mangostin isomer	80.43	1.05 ± 0.13^b	1.43 ± 0.17^c	0.53 ± 0.07^a	1.02 ± 0.11^b
X29	Garcinone B	80.78	0.21 ± 0.01^a	0.24 ± 0.03^a	n.d.	n.d.
X30	γ-Mangostin	81.11	0.30 ± 0.02^b	0.45 ± 0.03^c	n.d.	0.22 ± 0.02^a
X31	Garcinone E	81.70	1.99 ± 0.23^a	2.64 ± 0.32^b	2.32 ± 0.31^a	3.10 ± 0.35^b
X32	Xanthone derivative 7	82.56	n.d.	0.19 ± 0.01	n.d.	n.d.
X33	5-*O*-Methyl-2-deprenylrheediaxanthone B	82.60	n.d.	0.30 ± 0.02	n.d.	n.d.
X34	Xanthone derivative 8	83.08	n.d.	0.25 ± 0.03^a	0.48 ± 0.06^b	n.d.
X35	Xanthone derivative 9	83.65	0.12 ± 0.01^a	0.63 ± 0.04^c	n.d.	0.35 ± 0.02^b
X36	Cadensin G	84.16	n.d.	0.16 ± 0.01	n.d.	n.d.
X37	Garcinone C	84.20	0.32 ± 0.04^a	0.53 ± 0.03^b	0.51 ± 0.04^b	0.44 ± 0.05^{ab}
X38	Cadensin C isomer	84.65	0.25 ± 0.03^a	0.18 ± 0.02^a	0.35 ± 0.02^b	n.d.
Total			11.75 ± 1.26^a	18.02 ± 1.84^{bc}	14.37 ± 1.5^{ab}	10.86 ± 1.13^a

Note: Contents of xanthones are expressed as milligrams per gram dry weight (mg·g^{-1} DW ± SD). NTR: non-transformed roots; HR B, HR F, HR H: hairy root clones; n.d.: not detected; t_R: retention time. Values in one row marked with different lower-case letters denoted significant differences between samples ($p < 0.05$).

The xanthone derivative 6 (X15) and 1,3,7-trihydroxy-6-methoxy-8-prenyl xanthone isomer (X23) were *de novo* synthesized in all tested HR clones and the highest amounts of both xanthones were recorded in HR B. Six xanthones denoted as homomangiferin (X6), 3,6-dihydroxy-1,5,7-trimethoxy-xanthone (X20), 5-*O*-methyl-2-deprenylrheediaxanthone B (X33), cadensin G (X36), as well as xanthone derivatives 5 and 7 (X13 and X32, respectively) were *de novo* produced in HR B. Three xanthones identified as linixanthone C (X1), 2-isoprenylemodin (X7) and isomangiferin (X9) were exclusively found in HR H, while γ-mangostin isomer (X16) was evidenced only in HR F clone.

The quantitative analysis of xanthones showed markedly high variation between NTR and HR cultures. The clone HR B exhibited significantly higher amounts of γ-mangostin (X30) and its isomer (X28), garcinone E (X31), garcinone C (X37) and xanthone derivatives 4 and 9 (X10 and X35, respectively) compared to NTR. The γ-mangostin isomer (X27), garcinone C (X37), cadensin C isomer (X38), as well xanthone derivatives 1 and 4 (X2 and X10, respectively) were up-regulated in HR F in comparison to

control roots. The HR H demonstrated significantly elevated levels of linixanthone B (X8), γ-mangostin isomer (X27), garcinone E (X31) and xanthone derivatives 1, 4 and 9 (X2, X10 and X35, respectively) compared to NTR. Taking into account the total xanthone contents in root extracts, HR B was shown as a superior clone for accumulation of these compounds.

3.2 In Vitro Biological Activities of H. perforatum Root Extracts

3.2.1 Antidepressant Activity

Antidepressant activity of HR and control extracts through MAO-A inhibition is presented in Fig. 1A. The MAO-A inhibitory activity of NTR and HR B extracts at 250 µg·mL^{-1} was slightly elevated compared to HR H and HR F. Similarly, MAO-A inhibition by NTR and HR B at 150 µg·mL^{-1} was about 1.4-fold increased than HR H and HR F. The NTR extracts at 50 µg·mL^{-1} showed significantly increased MAO-A inhibition compared to HR. Root extracts at all tested concentrations showed decreased MAO-A inhibition compared to 2,4-DCP as a specific enzyme inhibitor.

3.2.2 Neuroprotective Activity

Neuroprotective activity of root extracts through AChE, BChE and tyrosinase inhibitory activity is shown in Figs. 1B–1D, respectively. The AChE inhibitory activity of HR F at 250 µg·mL^{-1} was slightly increased compared to the other root extracts. The variation in AChE inhibition between HR clones and NTR at other tested doses was not observed. Root extracts at all tested concentrations exhibited lower AChE inhibitory effect compared to eserine as a specific enzyme inhibitor.

The HR F extracts at 250 µg·mL^{-1} demonstrated significantly elevated BChE inhibition compared to the other transgenic lines and control roots. The BChE inhibitory activity of transgenic clones at 150 µg·mL^{-1} was about 1.5-fold increased in comparison to NTR. All tested root extracts showed comparable BChE inhibition at the lowest extract concentration. Nevertheless, all tested root samples demonstrated decreased BChE inhibitory activities compared to eserine.

Tyrosinase inhibitory activity of HR B at 250 µg·mL^{-1} was significantly elevated compared to the other transgenic clones and control roots. Similarly, HR B extracts at 150 µg·mL^{-1} displayed markedly increased tyrosinase inhibition compared to HR H (7.2-fold), as well to HR F and NTR (1.3-fold). The HR B clone at 50 µg·mL^{-1} showed a significantly higher capacity for tyrosinase inhibition compared to the other root extracts. Outgoing results demonstrated that HR B extract at all tested concentrations represented a powerful tyrosinase inhibitor. In spite of these results, all root samples demonstrated lower tyrosinase inhibition than kojic acid as a specific enzyme inhibitor.

3.2.3 Antidiabetic Activity

The antidiabetic activity of root extracts through α-amylase and α-glucosidase inhibition is presented in Figs. 1E and 1F, respectively. All transgenic clones at 250 µg·mL^{-1} showed significantly increased α-amylase inhibitory activity compared to NTR. The HR B extract at 150 µg·mL^{-1} exhibited slightly higher α-amylase inhibition compared to the other root extracts. Curiously, HR H and HR F clones at 50 µg·mL^{-1} displayed significantly elevated α-amylase inhibition compared to HR B and control. Despite these results, all root extracts showed lower α-amylase inhibitory activity than acarbose as a specific enzyme inhibitor.

The root extracts showed exceptionally high capacity for inhibition of α-glucosidase activity. The samples at 250 µg·mL^{-1} did not show any significant variation in α-glucosidase inhibitory activity. On the other hand, all HR extracts at 150 µg·mL^{-1} exhibited slightly increased α-glucosidase inhibition compared to NTR. The α-glucosidase inhibitory activity of HR at 50 µg·mL^{-1} was significantly enhanced compared to control roots. It is worth to point out that α-glucosidase inhibition by HR B and HR F clones at 250 µg·mL^{-1} was comparable to acarbose.
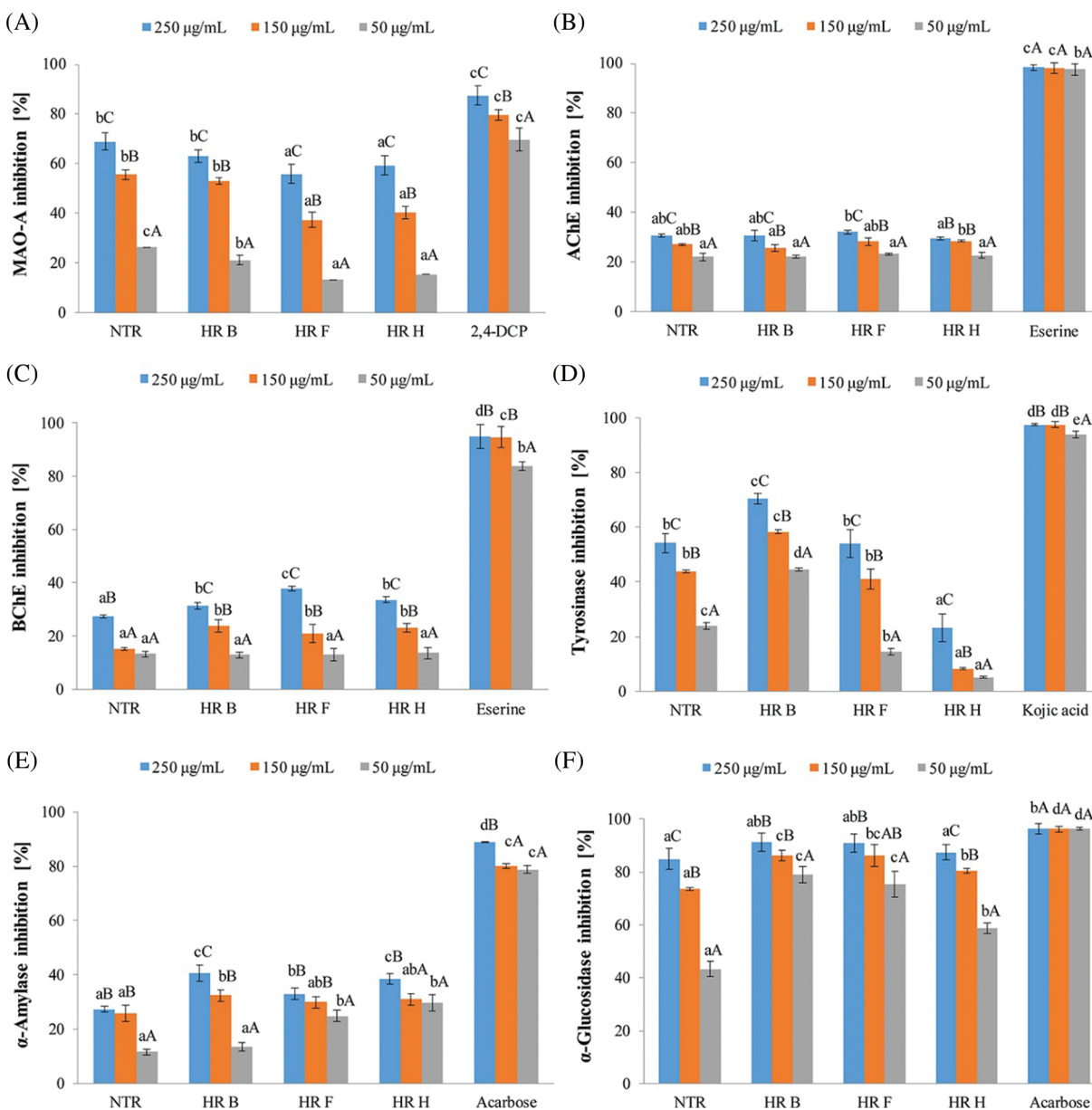
Figure 1: Inhibitory activity of *H. perforatum* root extracts against MAO-A (A), AChE (B), BChE (C), tyrosinase (D), α-amylase (E) and α-glucosidase (F). NTR: non-transformed roots; HR B, HR F, HR H: hairy root clones; 2,4-DCP: 2,4-dichlorophenol. The lower-case letters (a, b, c, d) showed significant differences ($p < 0.05$) between root extracts (NTR, HR B, HR F or HR H) within any particular concentration. The upper-case letters (A, B, C) showed significant differences ($p < 0.05$) between different concentrations (50, 150 or 250 μg·mL^{-1}) at any individual root extract

### 3.3 Molecular Modelling of Phenolic Compounds from H. perforatum Root Extracts

Molecular modelling was performed on five selected phenolic compounds (vanillic acid, epicatechin, quercetin 6-*C*-glucoside, mangiferin and γ-mangostin) due to their abundance in *H. perforatum* HR extracts. Molecular docking analyses revealed that those phenolic compounds have the capability to interact with different amino acid residues in the active site of the tested enzymes (MAO-A, AChE,

BChE, tyrosinase, α-amylase and α-glucosidase). Docking results concerning the binding energy and inhibition constant (K_i) between phenolic compounds and enzymes are presented in Table 3.

Table 3: Binding energy and inhibition constant of the best-ranked docking pose of selected ligands and enzymes

Ligands	Enzymes	Binding energy (kcal·mol^{-1})	Inhibition constant (K_i)
Vanillic acid	MAO-A	−5.35	119.97 μM
	AChE	−4.09	1.01 mM
	BChE	−4.26	758.48 μM
	Tyrosinase	−8.68	435.00 nM
	α-Amylase	−3.85	1.51 mM
	α-Glucosidase	−4.36	641.85 μM
Epicatechin	MAO-A	−8.30	817.30 nM
	AChE	−8.81	349.67 nM
	BChE	−8.55	544.48 nM
	Tyrosinase	−4.59	428.51 μM
	α-Amylase	−6.76	11.08 μM
	α-Glucosidase	−6.27	25.25 μM
Quercetin-6-*C*-glucoside	MAO-A	−4.82	294.12 μM
	AChE	−8.55	542.44 nM
	BChE	−6.27	25.25 μM
	Tyrosinase	−3.60	2.30 mM
	α-Amylase	−5.62	76.37 μM
	α-Glucosidase	−7.26	4.77 μM
Mangiferin	MAO-A	−5.16	164.87 μM
	AChE	−8.84	332.49 nM
	BChE	−6.48	17.91 μM
	Tyrosinase	−3.94	1.29 mM
	α-Amylase	−7.12	6.03 μM
	α-Glucosidase	−6.17	30.26 μM
γ-Mangostin	MAO-A	−9.97	49.35 nM
	AChE	−11.58	3.26 nM
	BChE	−10.08	41.12 nM
	Tyrosinase	−5.00	216.94 μM
	α-Amylase	−8.46	631.66 nM
	α-Glucosidase	−8.26	887.76 nM

Molecular docking data on MAO-A showed that phenolic compounds exhibited different binding energies towards the active cavity of the enzyme. The xanthone γ-mangostin displayed the best interaction with MAO-A enzymatic pocket (Fig. 2) that was represented with the lowest binding energy (−9.97 kcal·mol^{-1}). Its binding mode was established by two hydrogen bonds with amino acid residues Asn 181 and Phe 208, as well by several hydrophobic interactions with amino acids Phe 208 (π-π T-shaped), Tyr 407, Tyr 444 (π-π stacked) and the cofactor FAD (π-sigma).
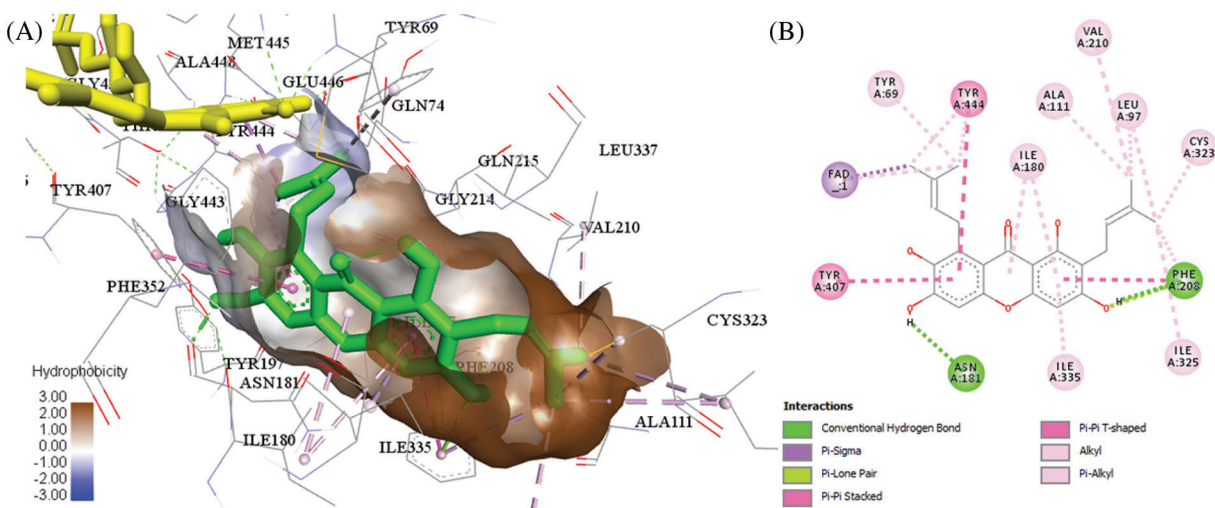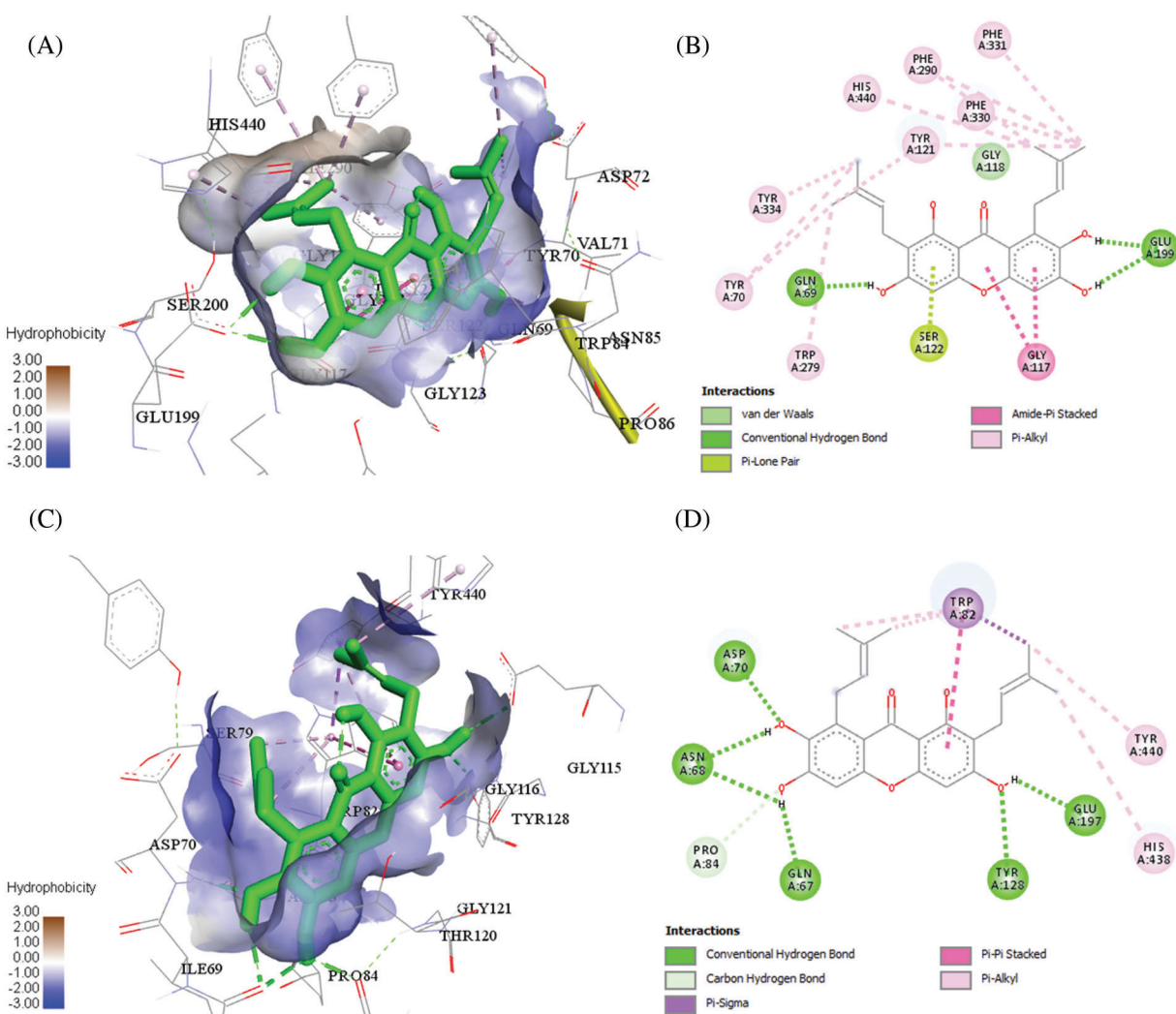
Figure 2: The best ranked docking pose (A) and key interactions (B) of γ-mangostin in the active site of MAO-A

The second potential interaction with MAO-A was found for epicatechin with a binding energy of −8.30 kcal·mol^{-1}. Namely, epicatechin binds into MAO-A active site by numerous hydrogen bonds with amino acid residues Asn 181, Phe 208, Thr 336 and Tyr 444. This ligand-enzyme complex was also stabilized by hydrophobic interactions with amino acid residues Ile 335 (π-sigma), Tyr 407 (π-π stacked) and FAD cofactor (π-π T-shaped). Other tested ligands showed moderate inhibition to MAO-A with binding energies ranging from −4.82 to −5.35 kcal·mol^{-1}.

Docking experiment on AChE revealed that γ-mangostin showed the best docking score with a binding energy of −11.58 kcal·mol^{-1}. The docking pose of γ-mangostin in the enzymatic pocket of AChE (Figs. 3A and 3B) was stabilized by formation of hydrogen bonds with amino acid residues Glu 199 (two interactions) and Gln 69, as well through two hydrophobic interactions with Gly 117 (π stacked). Favourable interactions in the enzymatic cavity of AChE were also found for quercetin 6-*C*-glucoside, epicatechin and mangiferin that exhibited comparable binding energy (−8.55, −8.81 and −8.84 kcal·mol^{-1}, respectively). The best docking pose for those ligands in the AChE active site was stabilized by interactions with the common amino acid residues Tyr 70, Asp 72, Trp 84 and Tyr 121. On the other hand, vanillic acid showed the lowest affinity towards AChE (binding energy −4.09 kcal·mol^{-1}) due to a limited number of non-bonding interactions with amino acid residues in the enzymatic cavity.

Concerning the docking study on BChE, γ-mangostin and epicatechin showed the best affinities to the enzyme active site (binding energies −10.08 and −8.55 kcal·mol^{-1}, respectively) through the establishment of strong interactions. The best docking pose of γ-mangostin into the BChE active center (Figs. 3C and 3D) was stabilized by the formation of numerous hydrogen bonds with amino acid residues Gln 67, Asn 68 (two interactions), Asp 70, Pro 84, Tyr 128 and Glu 197, as well as by two hydrophobic bonds with Gly 117. The best pose of epicatechin into the BChE enzyme pocket was represented with multiple hydrogen bonds to Gln 67, Asn 68 (two interactions), Asp 70, Asn 83, Gly 115, Glu 197 and His 438, as well by several hydrophobic interactions to Gly 115 and Gly 116 (π stacked), Trp 82 (π-π T-shaped) and Thr 120 (π-sigma). Other tested ligands exhibited moderate affinities to BChE and their binding energies ranged from −4.26 to −6.48 kcal·mol^{-1}.
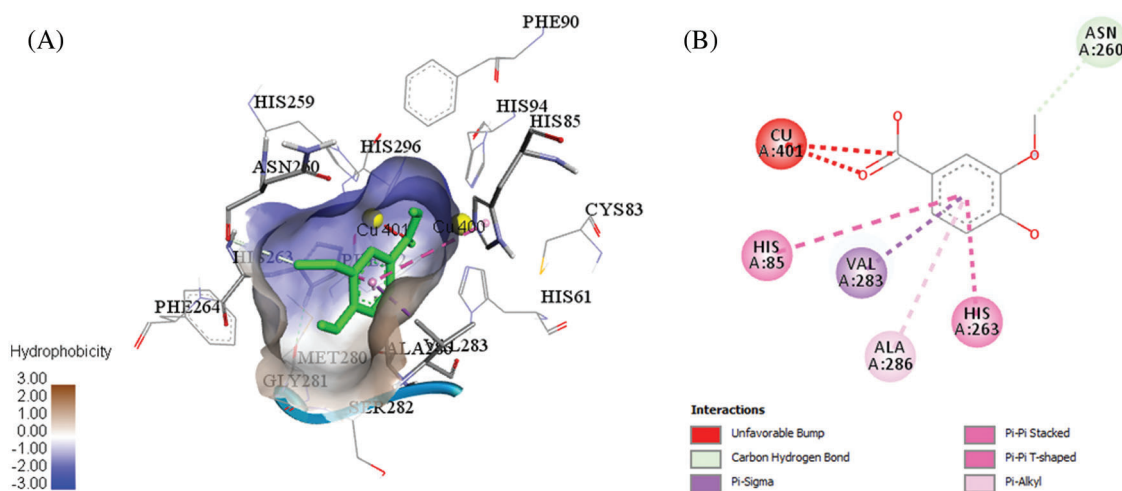
Figure 3: The best ranked docking pose (A) and key interactions (B) of γ-mangostin in the active site of AChE. The best ranked docking pose (C) and key interactions (D) of γ-mangostin in the active site of BChE

Docking results on tyrosinase showed that phenolic compounds exhibited various interactions with key amino acid residues that surround copper atoms in the enzymatic active site. It is interesting to point out that vanillic acid as the weakest inhibitor of MAO-A, AChE and BChE displayed the highest affinity toward tyrosinase (Fig. 4) with a binding energy of −8.68 kcal·mol^{-1}. In this context, vanillic acid-tyrosinase complex was stabilized by the formation of one hydrogen bond to Asn 260, several hydrophobic interactions to His 85 (π-π T-shaped), His 263 (π-π stacked) and Val 283 (π-sigma), as well as with two coordinative bonds involving Cu 401. In comparison to vanillic acid, other phenolic compounds exhibited low affinity to tyrosinase (binding energy from −3.60 to −5.00 kcal·mol^{-1}) that was evidenced by the scarcity of interactions with Cu atoms.

Molecular docking analysis on α-amylase demonstrated that γ-mangostin with a binding energy of −8.46 kcal·mol^{-1} was the most active phenolic compound providing various interactions in the enzyme active pocket (Figs. 5A and 5B). Its best docking pose was stabilized by three hydrogen bonds with amino acid residues Trp 59 and Glu 233 (two interactions). This complex of γ-mangostin and α-amylase was additionally stabilized by hydrophobic interactions involving Trp 58 and Tyr 62 (π–π T-shaped), as

well as Trp 59 (π-sigma). In addition, quercetin 6-*C*-glucoside, epicatechin and mangiferin exhibited low binding energies towards α-amylase (−5.62, −6.76 and −7.12 kcal·mol^{-1}, respectively). Those ligands showed the capability to interact with the common amino acid residues Trp 59, Asp 197 and Glu 233 (hydrogen bonds), as well as with Tyr 62 and Val 163 (hydrophobic interactions) in the α-amylase active site. In contrast, vanillic acid displayed the lowest affinity to α-amylase with a binding energy of −3.85 kcal·mol^{-1}.

Figure 4: The best ranked docking pose (A) and key interactions (B) of vanillic acid in the active site of tyrosinase

Docking calculations on phenolic compounds towards α-glucosidase were comparable to those observed for α-amylase with respect to their binding affinities (Figs. 5C and 5D). The best docking pose obtained for γ-mangostin on α-glucosidase (binding energy −8.26 kcal·mol^{-1}) was stabilized by forming hydrogen bonds to the amino acid residues Arg 213, Asp 215 and Asp 307 (two interactions), as well as by hydrophobic bonds to Tyr 72 (π-sigma) and Phe 303 (π-π stacked). The strong interactions towards α-glucosidase were also observed for quercetin 6-*C*-glucoside, epicatechin and mangiferin (binding energy from −6.17 to −7.26 kcal·mol^{-1}). The complexes of those ligands and the α-glucosidase active site were stabilized by several hydrogen and hydrophobic interactions that included the common amino acid residues Tyr 158, Phe 178 and Asp 215. Even vanillic acid showed the capacity for establishment of hydrogen bonds with various amino acids residues (Lys 156, Tyr 158, Ser 241 and Asp 242); this ligand was represented with the weakest affinity towards the α-glucosidase cavity (binding energy −4.36 kcal·mol^{-1}).

4 Discussion

4.1 Chromatographic Analysis of Phenolic Compounds

Identification of vanillic acid and syringic acid as hydroxybenzoic acids in transgenic and control roots was an important finding since the data for the presence of these compounds in the *H. perforatum* root extracts were rather scarce. According to the literature data, only vanillic acid has been detected in field- and *in vitro*-grown roots from *H. perforatum* subsp. *angustifolium* [8]. The confirmation of quinic acid in transgenic roots was expected because it has already been shown as the most common compound in *H. perforatum* HR cultures [17,22]. Even though our previous study revealed the presence of coumaroyl-, cafeoyl- and feruloyl-quinic acid derivatives in *H. perforatum* HR clones [18], these hydroxycinnamic acids were not confirmed here. The heterogeneity in phenolic acids profile in *H. perforatum* HR cultures

could be represented by the activation of a metabolic route that leads to the biosynthesis of vanillic acid and syringic acid from their corresponding hydroxycinnamic acids [36].
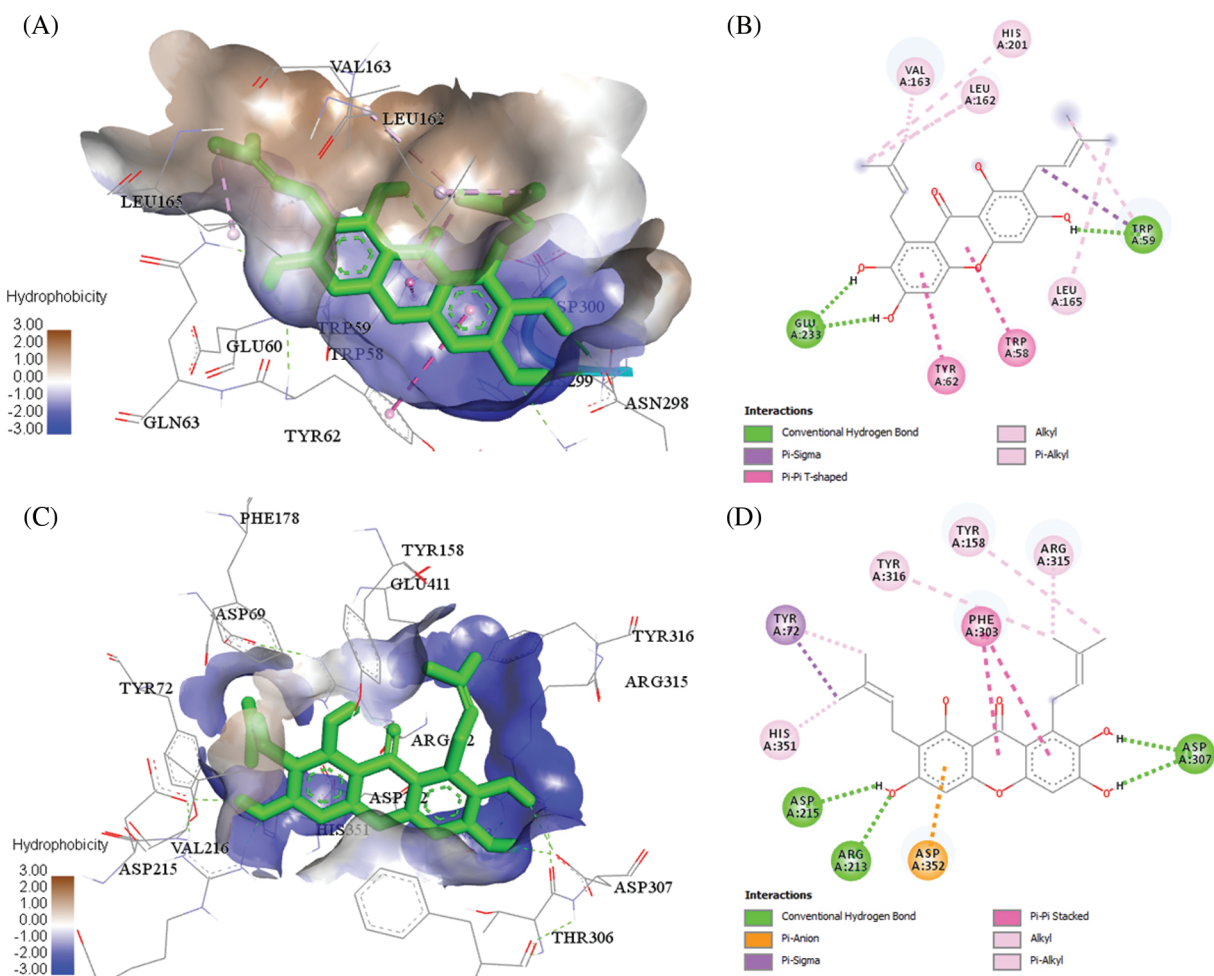
Figure 5: The best ranked docking pose (A) and key interactions (B) of γ-mangostin in the active site of α-amylase. The best ranked docking pose (C) and key interactions (D) of γ-mangostin in the active site of α-glucosidase

Catechins and procyanidins were represented as the major flavonoid fraction in *H. perforatum* root extracts. Comparatively, HR clones showed greater capability for the production of epicatechin than procyanidin derivatives. In this context, our previous studies showed that *H. perforatum* HR has a stronger capacity for accumulation of monomeric flavan-3-ols (catechin and epicatechin) than procyanidin derivatives [17,18]. These findings indicated that monomeric epicatechin may not be involved in the condensation reactions for the production of proanthocyanidins in HR. Taking into account the multibiological properties of epicatechin [37], *H. perforatum* transformed roots could be promoted as a novel biotechnological system for isolation of pharmacologically important compounds.

The present data showed that *H. perforatum* transgenic roots are a better source of quercetin 6-*C*-glucoside and kaempferol 6-*C*-glucoside than control roots. Such an increased accumulation of these two flavonols has already been observed in our recent study for *H. perforatum* liquid-grown HR [18]. In contrast, solid-grown *H. perforatum* HR accumulated lower amounts of quercetin 6-*C*-glucoside and they

did not exhibit any capacity for synthesis of kaempferol 6-*C*-glucoside [17]. This inconsistency in the results could be attributed to the influence of the culture media composition on the activity of enzymes involved in the accumulation of flavonol glucosides in HR cultures.

The chromatographic analysis clearly demonstrated that xanthones are prevailing phenolic compounds in *H. perforatum* root extracts. Among the identified xanthones, mangiferin, homomangiferin, γ-mangostin isomers and garcinone E were found as pre-eminent xanthones in transgenic clones. It has already been reported that production of xanthones in *Hypericum in vitro* roots could be manipulated by addition of phytohormones and elicitors or through genetic transformation [11–13,17,18]. Recent studies showed that genetic transformation of various *Hypericum* species with *A. rhizogenes* represented an efficient strategy for xanthone production in transgenic roots [12,17,18]. The HR cultures of *H. tetrapterum* and *H. tomentosum* have been proposed as a suitable system for production of 1,3,5,6- and 1,3,6,7-tetrahydroxyxanthone, biyouxanthone D, toxyloxanthone B and 1,7-dihydroxyxanthone [12]. From our previous studies on *H. perforatum* transgenic roots, trihydroxy-1-metoxy-*C*-prenyl xanthone has been found as a major compound along with different xanthones of 1,3,5,6- and 1,3,6,7-oxygenation pattern, mangiferin, γ-mangostin, toxyloxanthone, garcinone B, C and E, paxanthone B and cadensin G [17,18]. Outgoing results suggested that mangiferin and γ-mangostin represented the main chemical defense in transgenic roots due to the transformation with *Agrobacterium*. Additionally, xanthone biosynthesis in *H. perforatum* cell suspensions co-cultured with *A. tumefaciens* has been related by increased activity of benzophenone synthase [38]. Taken together, these compelling results support the hypothesis that xanthones belong to the defense arsenal employed by *H. perforatum* HR to combat biological stress factors due to the *Agrobacterium*-mediated transformation.

4.2 In Vitro Biological Activity and Molecular Modelling

4.2.1 Antidepressant Activity

The present data revealed that *H. perforatum* transgenic roots exhibited MAO-A inhibitory activity related to the accumulation of xanthones. We have already reported that xanthones from *H. perforatum* wild-growing roots are the main inhibitory compounds with MAO-A activity [3]. The effectiveness of xanthones for MAO-A inhibition has been correlated with para-oriented OH groups to the C=O function at the C3 and C6 positions, as well as prenyl substituents at the C2 and C8 positions [39,40]. Outgoing docking experiments showed that γ-mangostin as the representative of prenylated xanthones is the most prominent MAO-A inhibitor through the formation of hydrogen bonds and hydrophobic interactions into enzyme binding pocket. On the other hand, mangiferin as glycosylated xanthone exhibited lower affinity towards MAO-A due to a steric hindrance by glucose moiety that interrupt its fitting into the enzyme active site. In accordance, Gnerre et al. [39] have observed that mangiferin as *C*-glucosyl-xanthone was less active in MAO-A inhibition than its aglycone form (1,3,6,7-tetrahydroxyxanthone). Even docking results indicated that mangiferin is a weaker MAO-A inhibitor, its significant contents in HR extracts might additionally contribute to the antidepressant activity. From this study, *H. perforatum* transgenic roots could be presented as a sustainable system for large-scale production of xanthones with potential antidepressant activity.

4.2.2 Neuroprotective Activity

Outgoing results demonstrated that *H. perforatum* transgenic roots enriched in flavonols, flavan-3-ols and xanthones have a great capacity for cholinesterase and tyrosinase inhibition. From our previous study, *H. perforatum* wild-growing plants exhibited promising *in vitro* neuroprotective activity through AChE, BChE and tyrosinase inhibition and thus could be proposed as efficient natural remedies in the management of Alzheimer's and Parkinson's diseases [3]. Among the phenolic compounds used for docking analyses, γ-mangostin was found as the most potent inhibitor of AChE and BChE activities. The enzyme inhibition by γ-mangostin might be related to its capacity for establishment of hydrogen bonding

between OH group at the C7 position from aromatic ring A, as well as to the numerous hydrophobic interactions of C2 and C8 prenyl groups with amino acid residues from the enzyme active site. In this view, Khaw et al. [41] highlighted the importance of C7 hydroxyl and C8 prenyl groups from γ-mangostin for strong AChE and BChE inhibition. Docking results showed that mangiferin as glycosylated xanthone exhibited moderate affinity to AChE and BChE due to the lack of prenyl groups as prerequisite structures for cholinesterase inhibition. Molecular docking studies also revealed that flavan-3-ols and flavonol glycosides inhibited cholinesterases through multiple mode of interactions [42,43]. The strong binding affinity of epicatechin for AChE and BChE observed here could be attributed to the capability of OH groups for establishment of numerous hydrogen bonds with amino acid residues at the enzyme active site. Similarly, previous docking data have confirmed the cholinesterase inhibitory properties of catechin and epicatechin gallate [44,45]. With respect to flavonols, catechol group from aromatic ring B, as well as OH groups at C5 and C7 positions from ring A have been shown as the main contributors to the binding of quercetin ligands into the AChE and BChE active sites [46]. As presently established, those structural moieties of quercetin 6-C-glucoside were involved in the formation of hydrogen bonds with amino acid residues Asn 85 and Gly 116 from AChE and BChE enzymes. All these observations indicated that xanthones (γ-mangostin and mangiferin), flavan-3-ols (epicatechin, procyanidin dimers and procyanidin trimer) and flavonols (quercetin 6-C-glucoside) might greatly contribute to the neuroprotective potential of transgenic roots.

The phytochemical analyses showed that *H. perforatum* transgenic roots have the capability to accumulate phenolic compounds with tyrosinase inhibitory properties. Docking data revealed that vanillic acid was the most powerful tyrosinase inhibitor due to its capacity to interact with the enzyme Cu atoms. Similarly, tyrosinase inhibitory properties of vanillic acid derivatives have been related to their capacity for bond formation with Cu atoms and amino acid residues Asn 260, Val 283 and His 85 from the enzyme active center [47]. On the other hand, docking results showed that xanthone representatives (γ-mangostin and mangiferin) were weaker tyrosinase inhibitors compared to vanillic acid due to their incompetence to establish interactions with Cu atoms as the major enzyme cofactor. Even γ-mangostin and mangiferin showed low binding affinity, these xanthones can not be ruled out in tyrosinase inhibition due to their abundance in *H. perforatum* HR. This was supported by the evidence that the HR B clone with the highest tyrosinase inhibitory activity showed strong accumulation of prenylated xanthones, as well as *de novo* production of oxygenated xanthones. These results suggested that *H. perforatum* HR cultures represented an efficient source of vanillic acid and xanthones with promising antityrosinase properties that may additionally participate to the neuroprotective activity.

4.2.3 Antidiabetic Activity

To the best of our knowledge, this is the first report for the *in vitro* antihyperglycemic activity of *H. perforatum* HR through the inhibition of the carbohydrate-digesting enzymes α-amylase and α-glucosidase. Outgoing results demonstrated that HR clones enriched in xanthones exhibited a moderate α-amylase inhibitory activity that was evidenced by the highest binding affinity of γ-mangostin and mangiferin into the enzyme active site. Xanthone derivatives have already been reported as efficient inhibitors of α-amylase due to the capacity of OH groups at C3, C5, C6 and C7, as well as the prenyl side chains at C2 and C8 to adjust the xanthone nucleus in the center of V-shaped enzyme pocket [48]. In this context, docking results showed that γ-mangostin and mangiferin fulfil those characteristics that were essential for the establishment of hydrogen bonds with the amino acid residues Trp 59 and Glu 233 at the α-amylase active center.

The α-glucosidase inhibitory activity of HR clones was related to the accumulation of prenylated xanthones (γ-mangostin, garcinone C, garcinone E and 1,3,7-trihydroxy-6-metoxy-8-prenyl xanthone) and quercetin 6-C-glucoside. Present docking data clearly demonstrated that γ-mangostin is the best α-glucosidase inhibitor exhibiting a stable complex with the lowest binding energy. According to the

molecular docking studies, polyhydroxyl groups, prenylation patterns and expanded aromatic rings acted as key pharmacophores to form hydrogen bonds and π-π stacking interactions with α-glucosidase [49,50]. In addition, the effectiveness of xanthones as α-glucosidase inhibitors has been ascribed to the presence of prenyl substituents at C2 or C4 along with a hydroxyl group at C3 position. Thus, it could be assumed that prenylated xanthones detected in *H. perforatum* transgenic roots significantly affect α-glucosidase inhibitory activity. However, the contribution of quercetin 6-*C*-glucoside to the antihyperglycemic properties of HR could not be excluded, since it was selected as the second powerful inhibitor of α-glucosidase. In this context, flavonol glycosides with 2,3-double bond and ketone group at C4, as well as free OH group at C3 in the ring C have been reported as the most effective α-glucosidase inhibitors [51,52]. Even that quercetin 6-*C*-glucoside possesses these structural features, its glucose moiety may cause steric hindrance and limitation of binding interaction within the α-glucosidase active center due to increased molecular size and polarity [53]. It seems that α-glucosidase inhibitory activity of HR is more likely related to the substantial accumulation of xanthones rather than quercetin glycosides. All these findings suggested that antidiabetic activity of *H. perforatum* HR was influenced by the action of a particular compound or by synergistic effects of xanthones and flavonol glycosides.

5 Conclusion

This is the first study for integration of *in vitro* and *in silico* approaches to explain the contribution of certain phenolic compounds from *H. perforatum* hairy roots to the antidepressant, neuroprotective and antidiabetic activities. The phytochemical profile of transgenic roots revealed the presence of phenolic acids, flavan-3-ols, flavonol glycosides and xanthones that may be ascribed to the observed biological properties. Hairy root extracts were found to inhibit the tested enzymes related to depressive disorders (MAO-A), neurodegenerative diseases (AChE, BChE and tyrosinase) and diabetes (α-amylase and α-glucosidase). Molecular docking experiments on major phenolics such as vanillic acid, epicatechin, quercetin 6-*C*-glucoside, mangiferin and γ-mangostin provided new insights in their interactions with the enzyme active sites supporting the molecular basis of the biological activities of transgenic roots. The γ-mangostin as pre-eminent xanthone in transgenic roots showed the best binding affinity with the tested enzymes. In the long run, the evidence from *in vivo* animal and ADMET (absorption, distribution, metabolism, elimination, toxicity) studies may lead to understanding the potential efficacy of phenolic compounds from *H. perforatum* hairy roots as biologically active agents.

Authorship: OT, SGS and MT designed the experiments with *H. perforatum* hairy roots clones and performed biological activity and molecular docking analyses. JPS and MS analyzed phenolic compounds' contents. The manuscript was written by OT and SGS with contributions from all co-authors. All authors have read and approved the final version of the manuscript.

Conflicts of Interest: The authors declare that they have no conflicts of interest to report regarding the present study.

References
  1. Velingkar, V. S., Gupta, G. L., Hegde, N. B. (2017). A current update on phytochemistry, pharmacology and herb-drug interactions of *Hypericum perforatum*. *Phytochemistry Review, 16(4),* 725–744. DOI 10.1007/s11101-017-9503-7.
  2. Gioti, E. M., Fiamegos, Y. C., Skalkos, D. C., Stalikas, C. D. (2009). Antioxidant activity and bioactive components of the aerial parts of *Hypericum perforatum* L. from Epirus, Greece. *Food Chemistry, 117(3),* 398–404. DOI 10.1016/j.foodchem.2009.04.016.

3. Tusevski, O., Krstikj, M., Stanoeva, J. P., Stefova, M., Simic, S. G. (2018). Phenolic profile and biological activity of *Hypericum perforatum* L.: Can roots be considered as a new source of natural compounds? *South African Journal of Botany, 117,* 301–310. DOI 10.1016/j.sajb.2018.05.030.

4. Gadzovska, S., Maury, S., Delaunay, A., Spasenoski, M., Hagège, D. et al. (2013). The influence of salicylic acid elicitation of shoots, callus, and cell suspension cultures on production of naphtodianthrones and phenylpropanoids in *Hypericum perforatum* L. *Plant Cell, Tissue and Organ Culture, 113(1),* 25–39. DOI 10.1007/s11240-012-0248-0.

5. Bruni, R., Sacchetti, G. (2009). Factors affecting polyphenol biosynthesis in wild and field grown St. John's Wort (*Hypericum perforatum* L. Hypericaceae/Guttiferae). *Molecules, 14(2),* 682–725. DOI 10.3390/molecules14020682.

6. Carrubba, A., Lazzara, S., Giovino, A., Ruberto, G., Napoli, E. (2021). Content variability of bioactive secondary metabolites in *Hypericum perforatum* L. *Phytochemistry Letters, 46(2),* 71–78. DOI 10.1016/j.phytol.2021.09.011.

7. Crockett, S. L., Poller, B., Tabanca, N., Pferschy-Wenzig, E. M., Kunert, O. et al. (2011). Bioactive xanthones from the roots of *Hypericum perforatum* (common St John's wort). *Journal of the Science of Food and Agriculture, 91(3),* 428–434. DOI 10.1002/jsfa.4202.

8. Tocci, N., Simonetti, G., D'Auria, F. D., Panella, S., Palamara, A. T. et al. (2013a). Chemical composition and antifungal activity of *Hypericum perforatum* subsp. *angustifolium* roots from wild plants and plants grown under controlled conditions. *Plant Biosystems, 147(3),* 557–562. DOI 10.1080/11263504.2013.806964.

9. Goel, M. K., Kukreja, A. K., Bisht, N. S. (2009). *In vitro* manipulations in St. John's wort (*Hypericum perforatum* L.) for incessant and scale up micropropagation using adventitious roots in liquid medium and assessment of clonal fidelity using RAPD analysis. *Plant Cell, Tissue and Organ Culture, 96(1),* 1–9. DOI 10.1007/s11240-008-9453-2.

10. Brasili, E., Miccheli, A., Marini, F., Praticò, G., Sciubba, F. et al. (2016). Metabolic profile and root development of *Hypericum perforatum* L. *in vitro* roots under stress conditions due to chitosan treatment and culture time. *Frontiers in Plant Science, 7,* 507. DOI 10.3389/fpls.2016.00507.

11. Tocci, N., Simonetti, G., D'Auria, F. D., Panella, S., Palamara, A. T. et al. (2011). Root cultures of *Hypericum perforatum* subsp. *angustifolium* elicited with chitosan and production of xanthone-rich extracts with antifungal activity. *Applied Microbiology and Biotechnology, 91(4),* 977–987. DOI 10.1007/s00253-011-3303-6.

12. Zubrická, D., Mišianiková, A., Henzelyová, J., Valletta, A., de Angelis, G. et al. (2015). Xanthones from roots, hairy roots and cell suspension cultures of selected *Hypericum* species and their antifungal activity against *Candida albicans*. *Plant Cell Reports, 34(11),* 1953–1962. DOI 10.1007/s00299-015-1842-5.

13. Tocci, N., D'Auria, F. D., Simonetti, G., Panella, S., Palamara, A. T. et al. (2013b). Bioassay-guided fractionation of extracts from *Hypericum perforatum in vitro* roots treated with carboxymethylchitosans and determination of antifungal activity against human fungal pathogens. *Plant Physiology and Biochemistry, 70,* 342–347. DOI 10.1016/j.plaphy.2013.05.046.

14. Valletta, A., de Angelis, G., Badiali, C., Brasili, E., Miccheli, A. et al. (2016). Acetic acid acts as an elicitor exerting a chitosan-like effect on xanthone biosynthesis in *Hypericum perforatum* L. root cultures. *Plant Cell Reports, 35(5),* 1009–1020. DOI 10.1007/s00299-016-1934-x.

15. Hou, W., Shakya, P., Franklin, G. (2016). A perspective on *Hypericum perforatum* genetic transformation. *Frontiers in Plant Science, 7(265),* 879. DOI 10.3389/fpls.2016.00879.

16. Vinterhalter, B., Ninković, S., Cingel, A., Vinterhalter, D. (2006). Shoot and root culture of *Hypericum perforatum* L. transformed with *Agrobacterium rhizogenes* A4M70GUS. *Biologia Plantarum, 50(4),* 767–770. DOI 10.1007/s10535-006-0127-9.

17. Tusevski, O., Stanoeva, J. P., Stefova, M., Kungulovski, D., Pancevska, N. A. et al. (2013a). Hairy roots of *Hypericum perforatum* L.: A promising system for xanthone production. *Open Life Sciences, 8(10),* 1010–1022. DOI 10.2478/s11535-013-0224-7.

18. Tusevski, O., Vinterhalter, B., Milošević, D. K., Soković, M., Ćirić, A. et al. (2017). Production of phenolic compounds, antioxidant and antimicrobial activities in hairy root and shoot cultures of *Hypericum perforatum* L. *Plant Cell, Tissue and Organ Culture, 128(3),* 589–605. DOI 10.1007/s11240-016-1136-9.

19. Vinterhalter, B., Zdravković-Korać, S., Mitić, N., Bohanec, B., Vinterhalter, D. et al. (2015). Effect of sucrose on shoot regeneration in *Agrobacterium* transformed *Hypericum perforatum* L. roots. *Acta Physiologiae Plantarum, 37(2),* 1–12. DOI 10.1007/s11738-015-1785-z.

20. Tusevski, O., Stanoeva, J. P., Stefova, M., Spasenoski, M., Simic, S. G. (2019). State of antioxidant systems and phenolic compounds' production in *Hypericum perforatum* L. hairy roots. *Acta Physiologiae Plantarum, 41(8),* 1–15. DOI 10.1007/s11738-019-2919-5.

21. Komarovská, H., Košuth, J., Giovannini, A., Smelcerovic, A., Zuehlke, S. et al. (2010). Effect of the number of *rol* genes integrations on phenotypic variation in hairy root-derived *Hypericum perforatum* L. plants. *Zeitschrift für Naturforschung C, 65(11–12),* 701–712. DOI 10.1515/znc-2010-11-1211.

22. Tusevski, O., Stanoeva, J. P., Stefova, M., Simic, S. G. (2013). Phenolic profile of dark-grown and photoperiod-exposed *Hypericum perforatum* L. hairy root cultures. *The Scientific World Journal, 2013*. DOI 10.1155/2013/602752.

23. Tusevski, O., Stanoeva, J. P., Stefova, M., Pavokovic, D., Simic, S. G. (2014). Identification and quantification of phenolic compounds in *Hypericum perforatum* L. transgenic shoots. *Acta Physiologiae Plantarum, 36(10),* 2555–2569. DOI 10.1007/s11738-014-1627-4.

24. Berman, H. M., Westbrook, Z., Feng, G., Gilliland, T. N., Bhat, H. et al. (2000). The protein data bank. *Nucleic Acid Research, 28(1),* 235–242. DOI 10.1093/nar/28.1.235.

25. Son, S. Y., Ma, J., Kondou, Y., Yoshimura, M., Yamashita, E. et al. (2008). Structure of human monoamine oxidase A at 2.2-Å resolution: The control of opening the entry for substrates/inhibitors. *PNAS, 105(15),* 5739–5744. DOI 10.1073/pnas.0710626105.

26. Pesaresi, A., Lamba, D. (2016). Torpedo Californica acetylcholinesterase in complex with a tacrine-nicotinamide hybrid inhibitor. *Protein Data Bank*. DOI 10.2210/pdb4x3c/pdb.

27. Nachon, F., Brazzolotto, X., Trovaslet, M., Masson, P. (2013). Progress in the development of enzyme-based nerve agent bioscavengers. *Chemico-Biologocial Interactions, 206(3),* 536–544. DOI 10.1016/j.cbi.2013.06.012.

28. Ismaya, W. T., Rozeboom, H. J., Schurink, M., Boeriu, C. G., Wichers, H. et al. (2011). Crystallization and preliminary X-ray crystallographic analysis of tyrosinase from the mushroom *Agaricus bisporus*. *Acta Crystallographica Section F, 67(5),* 575–578. DOI 10.1107/S174430911100738X.

29. Zhuo, H., Payan, F., Qian, M. (2004). Crystal structure of the pig pancreatic α-amylase complexed with ρ-nitrophenyl-α-d-maltoside-flexibility in the active site. *The Protein Journal, 23(6),* 379–387. DOI 10.1023/B:JOPC.0000039552.94529.95.

30. Yamamoto, K., Miyake, H., Kusunoki, M., Osaki, S. (2011). Steric hindrance by 2 amino acid residues determines the substrate specificity of isomaltase from *Saccharomyces cerevisiae*. *Journal of Bioscience and Bioengineering, 112(6),* 545–550. DOI 10.1016/j.jbiosc.2011.08.016.

31. Morris, G. M., Huey, R., Lindstrom, W., Sanner, M. F., Belew, R. K. et al. (2009). AutoDock4 and AutoDockTools4: Automated docking with selective receptor flexibility. *Journal of Computational Chemistry, 30(16),* 2785–2791. DOI 10.1002/jcc.21256.32.

32. Chen, V. B., Arendall, W. B., Headd, J. J., Keedy, D. A., Immormino, R. M. et al. (2010). MolProbity: All-atom structure validation for macromolecular crystallography. *Acta Crystallographica Section D, 66(1),* 12–21. DOI 10.1107/S0907444909042073.

33. Kim, S., Chen, J., Cheng, T., Gindulyte, A., He, J. et al. (2019). PubChem in 2021: New data content and improved web interfaces. *Nucleic Acids Research, 49(D1),* D1388–D1395. DOI 10.1093/nar/gkaa971.

34. ACD/Chemsketch Ver. 12.0 (2009). Advanced Chemistry Development, Inc. Toronto, Canada.

35. Pedretti, A., Villa, L., Vistoli, G. (2004). VEGA-An open platform to develop chemo-bio-informatics applications, using plug-in architecture and script programming. *Journal of Computer-Aided Molecular Design, 18(3),* 167–173. DOI 10.1023/B:JCAM.0000035186.90683.f2.

36. El-Basyouni, S. Z., Neish, A. C., Towers, G. H. N. (1963). The phenolic acids in wheat–III.: Insoluble derivatives of phenolic cinnamic acids as natural intermediates in lignin biosynthesis. *Phytochemistry, 3(6),* 627–639. DOI 10.1016/S0031-9422(00)82960-X.

37. Prakash, M., Basavaraj, B. V., Murthy, K. C. (2019). Biological functions of epicatechin: Plant cell to human cell health. *Journal of Functional Foods, 52(4),* 14–24. DOI 10.1016/j.jff.2018.10.021.

38. Franklin, G., Conceição, L. F., Kombrink, E., Dias, A. C. (2009). Xanthone biosynthesis in *Hypericum perforatum* cells provides antioxidant and antimicrobial protection upon biotic stress. *Phytochemistry, 70(1),* 60–68. DOI 10.1016/j.phytochem.2008.10.016.

39. Gnerre, C., Poser, G. L., Ferraz, A., Viana, A., Testa, B. et al. (2001). Monoamine oxidase inhibitory activity of some *Hypericum* species native to South Brazil. *Journal of Pharmacy and Pharmacology, 53(9),* 1273–1279. DOI 10.1211/0022357011776568.

40. Dhiman, P., Malik, N., Khatkar, A. (2018). 3D-QSAR and *in-silico* studies of natural products and related derivatives as monoamine oxidase inhibitors. *Current Neuropharmacology, 16(6),* 881–900. DOI 10.2174/1570159X15666171128143650.

41. Khaw, K. Y., Choi, S. B., Tan, S. C., Wahab, H. A., Chan, K. L. et al. (2014). Prenylated xanthones from mangosteen as promising cholinesterase inhibitors and their molecular docking studies. *Phytomedicine, 21(11),* 1303–1309. DOI 10.1016/j.phymed.2014.06.017.

42. Katalinić, M., Rusak, G., Barović, J. D., Šinko, G., Jelić, D. et al. (2010). Structural aspects of flavonoids as inhibitors of human butyrylcholinesterase. *European Journal of Medicinal Chemistry, 45(1),* 186–192. DOI 10.1016/j.ejmech.2009.09.041.

43. Zengin, G., Mollica, A., Aumeeruddy, M. Z., Rengasamy, K. R., Mahomoodally, M. F. (2018). Phenolic profile and pharmacological propensities of *Gynandriris sisyrinchium* through *in vitro* and *in silico* perspectives. *Industrial Crops and Products, 121,* 328–337. DOI 10.1016/j.indcrop.2018.05.027.

44. Zengin, G., Ceylan, R., Katanić, J., Mollica, A., Aktumsek, A. et al. (2017). Combining *in vitro*, *in vivo* and *in silico* approaches to evaluate nutraceutical potentials and chemical fingerprints of *Moltkia aurea* and *Moltkia coerulea*. *Food and Chemical Toxicology, 107,* 540–553. DOI 10.1016/j.fct.2017.04.004.

45. Li, F. J., Liu, Y., Yuan, Y., Yang, B., Liu, Z. M. (2017). Molecular interaction studies of acetylcholinesterase with potential acetylcholinesterase inhibitors from the root of *Rhodiola crenulata* using molecular docking and isothermal titration calorimetry methods. *International Journal of Biological Macromolecules, 104,* 527–532. DOI 10.1016/j.ijbiomac.2017.06.066.

46. Ji, H. F., Zhang, H. Y. (2006). Theoretical evaluation of flavonoids as multipotent agents to combat Alzheimer's disease. *Journal of Molecular Structure: THEOCHEM, 767(1–3),* 3–9. DOI 10.1016/j.theochem.2006.04.041.

47. Nazir, Y., Saeed, A., Rafiq, M., Afzal, S., Ali, A. et al. (2020). Hydroxyl substituted benzoic acid/cinnamic acid derivatives: Tyrosinase inhibitory kinetics, anti-melanogenic activity and molecular docking studies. *Bioorganic & Medicinal Chemistry Letters, 30(1),* 126722. DOI 10.1016/j.bmcl.2019.126722.

48. Ibrahim, S. R. M., Mohamed, G. A., Khayat, M. T. A., Ahmed, S., Abo-Haded, H. (2019). α-amylase inhibition of xanthones from *Garcinia mangostana* pericarps and their possible use for the treatment of diabetes with molecular docking studies. *Journal of Food Biochemistry, 43(5),* e12844. DOI 10.1111/jfbc.12844.

49. Fouotsa, H., Lannang, A. M., Mbazoa, C. D., Rasheed, S., Marasini, B. P. et al. (2012). Xanthones inhibitors of α-glucosidase and glycation from *Garcinia nobilis*. *Phytochemistry Letters, 5(2),* 236–239. DOI 10.1016/j.phytol.2012.01.002.

50. Liu, Y., Ma, L., Chen, W. H., Park, H., Ke, Z. et al. (2013). Binding mechanism and synergetic effects of xanthone derivatives as noncompetitive α-glucosidase inhibitors: A theoretical and experimental study. *The Journal of Physical Chemistry B, 117(43),* 13464–13471. DOI 10.1021/jp4067235.

51. Rastija, V., Bešlo, D., Nikolić, S. (2012). Two-dimensional quantitative structure-activity relationship study on polyphenols as inhibitors of α-glucosidase. *Medicinal Chemistry Research, 21(12),* 3984–3993.

52. Das, K., Mohammed, S., Khan, M. S., Singirikonda, S., Alamri, A. S. et al. (2022). Phytochemical analysis, estimation of quercetin, and *in vitro* anti-diabetic potential of stevia leaves samples procured from two geographical origins. *Phyton-International Journal of Experimental Botany, 91(10),* 2349–2365. DOI 10.32604/phyton.2022.022379.

53. Hua, F., Zhou, P., Wu, H. Y., Chu, G. X., Xie, Z. W. et al. (2018). Inhibition of α-glucosidase and α-amylase by flavonoid glycosides from Lu'an GuaPian tea: Molecular docking and interaction mechanism. *Food & Function, 9(8),* 4173–4183. DOI 10.1039/C8FO00562A.